Engineering Structures 353 (2026) 122191

Contents lists available at ScienceDirect

Engineering Structures

journal homepage: www.elsevier.com/locate/engstruct

From lab to blade: Scalable validation of a durable silicone-epoxy icephobic coating for wind turbine blades

Ghazal Minoofar [a,*], Gelareh Momen [a,b], Thomas Allard [a], Derek Harvey [a], Eric Villeneuve [c], Reza Jafari [a]

[a] Department of Applied Sciences, University of Quebec in Chicoutimi (UQAC), 555, boul. de l'Université, Chicoutimi, Quebec G7H 2B1, Canada
[b] Department of Aerospace Engineering, École de Technologie Supérieure (ÉTS)1100 Notre-Dame Rue O, Montreal, Quebec H3C 1K3, Canada
[c] Department of Mathematics, Computer Science and Engineering, University of Quebec at Rimouski (UQAR), 300, allée des Ursulines CP 3300, succ. A, Rimouski, Quebec G5L 3A1, Canada

ARTICLE INFO

Keywords:
Wind-turbine Anti-icing
Passive methods
Icephobic surface coatings
Large-scale performance evaluation
Silicone-epoxy coating

ABSTRACT

Ice accumulation on large rotor blades poses a major operational challenge by reducing energy output and threatening structural integrity. Active de-icing systems are effective but limited by high energy demand, delayed response, and elevated costs. Passive solutions, particularly silicone–epoxy icephobic coatings, offer advantages such as low surface energy, durability, and reduced ice adhesion, enabling earlier shedding. However, most studies remain confined to laboratory scale without validation under realistic conditions. This study addresses this gap by evaluating a durable commercial silicone–epoxy coating at both laboratory and large scales. Laboratory characterization following ISO/TS 19392 standards showed a water contact angle of 100° ± 2.2°, mechanical abrasion resistance of 72 ± 2.1 mg/1000, and ice adhesion strength below 20 kPa even after 50 icing/de-icing cycles, confirming strong icephobic performance. Push-off and CAT tests with short ice specimens predominantly exhibited adhesion-dominated detachment, favorable for anti-icing. In contrast, spinning rotor blade and field trials with more realistic accretions often resulted in cohesive or mixed failures, leaving residual ice. These results indicate that adhesion-focused behavior observed in small-scale tests correlates with the more complex detachment dynamics at larger scales, demonstrating how laboratory measurements can predict expected performance and benefits under operational conditions. Overall, the study demonstrates the value of integrating quantitative material properties with multi-scale adhesion testing to guide the design of ice-mitigation coatings. In practice, the coating's role is best understood as part of broader ice protection strategies, where variables such as rotation speed during accretion strongly influence shedding.

1. Introduction

The growing demand for renewable energy has established wind turbines as essential components in the global shift towards sustainable power sources [1]. The performance of wind turbines improves as the temperature decreasesbecause colder air is denser, allowing the turbine to capture more energy from the wind [2,3], however, a significant challenge these turbines face is the accumulation of ice on their blades, which can severely hinder aerodynamic performance, reduce energy efficiency, and compromise operational reliability [4–6]. While several active anti-icing methods, such as electro-thermal heating, hot air circulation, and mechanical de-icing systems, have been designed and employed to address this issue, they often suffer from high energy consumption, increased operational complexity, and maintenance demands, especially under harsh environmental conditions [5,7,8]. To mitigate this issue, the advancement of anti-icing coatings has become a key focus in addressing ice accumulation on wind turbine blades due to zero emission benefits, operational costs and energy usage. To be effective, anti-icing coatings designed for wind turbines need to satisfy several critical performance requirements [9,10]. Mechanical robustness is essential, as the coatings must endure environmental and operational stresses, including wind-induced forces, blade elongation, and bending. Standards such as ISO 527–1, ASTM D2240, and ASTM D4060 are commonly used to evaluate tensile strength, hardness, and abrasion

* Corresponding author.
E-mail addresses: ghazal.minoofar2@gmail.com (G. Minoofar), Gelareh_Momen@uqac.ca (G. Momen), tallard1@etu.uqac.ca (T. Allard), d2harvey@uqac.ca (D. Harvey), eric_villeneuve@uqar.ca (E. Villeneuve), Reza_Jafari@uqac.ca (R. Jafari).

https://doi.org/10.1016/j.engstruct.2026.122191
Received 27 September 2025; Received in revised form 15 December 2025; Accepted 17 January 2026
Available online 20 January 2026

resistance, respectively, ensuring the durability of coatings under such conditions [11–13]. In addition to mechanical performance, these coatings must exhibit high icephobicity to minimize ice accumulation and adhesion, critical for maintaining aerodynamic efficiency and reducing maintenance needs. This is assessed according to ISO/TS 19392–6:2023, which provides testing guidelines for icephobic properties in wind turbine applications [14]. Rain erosion resistance is another critical factor; coatings need to withstand impacts from water droplets that can strike blade tips at speeds nearing 90 m/s on large wind turbines (ISO/TS 19392–3) [15]. Additionally, abrasion resistance is essential for maintaining performance under harsh environmental conditions [16]. These characteristics are largely determined by the polymer selected as the base resin [17–19]. Among polymer-based resins, silicone-epoxy coatings stand out for their superior performance, particularly in harsh environmental conditions, due to the synergistic combination of the unique properties of both silicone and epoxy. The silicone component imparts low surface energy to the coating, which plays a crucial role in reducing ice adhesion strength (τice) by weakening bonding forces between the ice and the surface [20]. This also contributes to low wettability, minimizing water accumulation and promoting droplet roll-off, factors that further enhance icephobic behavior. Meanwhile, the epoxy component provides mechanical robustness, strong adhesion to various substrates, and resistance to wear and environmental degradation [21], resulting in coatings that are not only durable but also highly icephobic. As a result, silicone-epoxy coatings are especially interesting for applications where resistance to ice accumulation and ease of ice removal are essential for maintaining operational reliability in subzero environments [22,23]. However, despite their promising potential, these coatings face challenges such as limited large-scale validation, susceptibility to mechanical damage under harsh icing conditions, and potential degradation over long-term field exposure. Consequently, studies on the anti-icing performance of silicone-epoxy coatings remain relatively few, with development efforts concentrated in a small number of research groups [24–26]. Typically, these researchers employ a range of methodologies to enhance the icephobic properties of silicone-epoxy resins, as detailed below. For example, Adja et al. [27] recently fabricated an icephobic silicone–epoxy hybrid coating using commercial silicone–epoxy resins (SILIKOPON® EF & ED), two fluorinated silicone additives, and amino-functional silane-curing agents for steel substrates. They reported an τice for 94 kPa. Further research [28] examined the anti-/de-Icing performance of epoxy coatings with GO-PPy@SiO_2 as photothermal fillers. The researchers claimed that at an optimal filler concentration, the water droplet on their produced coating remained unfrozen for 710 s at −15°C, effectively delaying icing. Also, when their sample was exposed to simulated sunlight, the surface temperature of the coating rapidly increased from room temperature to over 80 °C within 10 min, peaking at 84.9°C, resulting in frozen droplets melting within just 5 s. Ziętkowska et al. [29] tailored a commercial silicone-epoxy resin (SILIKOPON® ED) through the incorporation of dually functionalized polysiloxanes to fabricate icephobic coatings for photovoltaic panel utilizations. They found that the chemical modification significantly improved the icephobicity of the prepared coatings with a 69 % decrease τice (reaching below 100 kPa) and 17 times increase in the freezing delay time in comparison with the pure ones. The silicon-epoxy coatings showed a contact angle hysteresis (CAH) of 7° to 11° and a roll-off angle of 32° to 55°. Following the approach of Zhao et al. [30] a robust icephobic coating was developed using an interpenetrating polymer network (IPN) of epoxy and Polydimethylsiloxane (PDMS). Low-molecular-weight silicone oil was also incorporated to reduce the crosslink density, allowing precise control of the coating's elastic modulus. This adjustment contributed to achieving optimal icephobic properties by balancing low ice adhesion and coating strength. Testing demonstrated that the coating's τice reached approximately 8 kPa at an elastic modulus of 0.18 MPa. Even after 25 cycles of icing and de-icing, the coating remained stable, with τice consistently maintained between 3 and 14 kPa. In another study, Sullivan et al. [31] designed a dual-function anti-icing system featuring a superhydrophobic layer supported by an embedded thin-film heating element. After 52 s heating, the SiO_2-PDMS coating exhibited rapid thermal response up to 60 °C. It also showed superhydrophobicity with a 164° contact angle and 3° hysteresis. In cold chamber tests, the hybrid coating reduced ice adhesion by 83 % (from 284 kPa to 50 kPa) and delayed freezing, achieving full anti-icing with 0.34 W/cm^2 power density, reducing energy consumption by 37 %. Zhang et al. [32] fabricated a durable, anti-corrosive superhydrophobic coating with photothermal properties, made with Fe_3O_4 composite nanoparticles in dual sizes (200 nm and 20 nm) for anti-icing and de-icing applications, which was sprayed onto glass substrates. The coating,), PDMS as a protective layer, and epoxy as the basecoat, uses Fe_3O_4 NPs optimized to achieve superior micro/-nanostructures. This design enhances photothermal conversion under simulated sunlight with a radiation intensity of 1 kW/m^2, achieving a heating rate of 14.4 °C/min and a light-to-heat conversion efficiency of 62.38 %. [33].

Despite extensive research on various icephobic materials, a significant gap remains in translating laboratory findings into real-world applications, particularly for wind turbine blades exposed to dynamic, harsh, and variable environmental conditions [34,35]. Most studies have been limited to small-scale tests [36] on flat, idealized surfaces under simplified icing conditions, often leading to complete ice detachment due to short interface lengths and purely adhesive failure modes, where the bond between the ice and the substrate fails at the ice/substrate interface [37,38]. However, real-world ice accretion involves both adhesive and cohesive failures (the ice itself fractures and breaks apart internally) across much longer spans [39,40]. In operational turbines, ice buildup reduces rotational speed (RPM), diminishing the centrifugal forces essential for passive ice shedding, especially against dense ice types like glaze or hard rime, where gravity or aerodynamic forces are typically insufficient. While full-span shedding is ideal, the outer third of the blade is particularly critical, as it contributes most to lift and energy output. Low τice measured in the lab can support passive shedding by allowing centrifugal and aerodynamic forces to remove ice more easily, potentially improving energy production, reducing downtime, and lowering maintenance costs, though its effectiveness depends heavily on in-field conditions. This study aims to bridge this lab-to-field gap by evaluating a commercially available silicone-epoxy coating (Lotus Dry) from our industrial partner, Techeol, Canada, under realistic geometries, ice types, and mechanical stresses to assess its practical ice-shedding performance on wind turbine blades.

The study is structured in two phases: the first phase involved detailed laboratory characterization of the silicone-epoxy coating, with various tests conducted to assess their icephobic, mechanical and durability properties. The second phase transitioned from small-scale laboratory characterization to larger scale realistic testing by applying the coatings on 1.3 m radius × 2.6 m long rotor blades installed in a 12 m high cold room, to evaluate their performance under simulated atmospheric icing conditions. This approach takes into account environmental factors such as droplet size, liquid water content, wind speed, and precipitation intensity, providing a comprehensive understanding of the coatings' effectiveness in mitigating ice accumulation on wind turbines.

This dual-scale investigation, by examining both laboratory characterization and large-scale applications, offers a deeper understanding of how these coatings can be optimized to address the challenges faced by wind turbines in cold climates, while also demonstrating the correlation between lab-scale and larger-scale more representative tests, ultimately contributing to improved performance and energy efficiency.

2. Materials and methods

2.1. Material

The commercial silicone-epoxy coating (Lotus Dry), used as the primary topcoat in this study, was obtained from Techeol, Canada. This coating was selected for its advertised hydrophobicity and weather resistance, highlighting its potential as a candidate for improving the surface durability under harsh environmental conditions. As the base layer and reference for comparative analysis, a polyester gel coat (VIBRIN G290AA) supplied by AOC was applied. This specific gel coat was chosen because it is commonly used in industry as a protective layer on fiberglass-epoxy composite wind turbine blades. Its established performance and compatibility with composite substrates make it an ideal benchmark for evaluating the enhancements offered by the silicone-epoxy topcoat.

2.2. Sample preparation

In this study, specimen preparation methods were tailored to the specific requirements of each test, considering variations in geometry, surface conditions, and coating application. Detailed preparation procedures are provided in the respective sections corresponding to each test. All aluminium substrates used were first cleaned with acetone to remove surface contaminants and then pre-coated with a polyester gelcoat (VIBRIN G290AA). Aluminum is widely used in aerospace, and other engineering components. Testing on aluminum provides results that are closer to what would be expected in real-world applications. The gelcoat layer was allowed to fully cure at room temperature for three days. Subsequently, the silicone-epoxy topcoat (Lotus Dry) was spray-applied onto the cured gelcoat surface and allowed to fully cure at room temperature for seven days. The average dry thickness of the gelcoat and coating were approximately 400 ± 20 μm, measured using DeFelsko's PosiTector 200 and Elektrophysik MiniTest70 coating thickness gauges.

2.3. Surface characterization

Water Contact Angle (WCA) and contact angle hysteresis (CAH) were measured to evaluate surface wettability. A Kruss™ DSA100 goniometer at 25 ± 0.5 °C was used with the sessile drop technique. In this method, a 4 μL water droplet was dropped on the surface, and WCA was calculated using the Young–Laplace model. The sliding angle (SA) of water droplets was evaluated using a Krüss instrument equipped with a tilting platform. Each sample was securely mounted on the stage, and a 35 μL water droplet, selected to minimize gravitational effects [41], was deposited on its surface before the stage was gradually inclined at a rate of 60° per minute up to a maximum of 60°, until the droplet-initiated sliding or rolling. The sliding angle was recorded as the stage inclination measured 0.5 s before the droplet began to move. Additionally, CAH was calculated by inclining and subtracting the receding contact angle from the advancing contact angle. These measurements helped to evaluate how the surface interacted with water, reflecting its hydrophobic properties.

2.4. Evaluation of the mechanical durability of the coating

A variety of tests were conducted to assess the mechanical durability of the coating, including tensile testing, rain erosion, and abrasion resistance. These assessments aimed to evaluate the coating's mechanical durability, wear resistance, and stability under simulated environmental conditions.

2.4.1. Tensile strength

A tensile test is a key method for evaluating the mechanical properties of the coating, specifically its tensile strength, elongation, and flexibility. In this test, according to ISO/TS 19392–1, five free films of the coating were subjected to a controlled, uniaxial force until failure, providing essential data on the material's ability to resist deformation and fracture under stress at room temperature. Additionally, five free films of the Lotus Dry were tested at low temperature (-35°C) to assess the coating's performance under varying thermal conditions.

2.4.2. Rain erosion

Wind turbines are constantly subjected to high-velocity rain, which can cause significant wear on their surfaces, potentially leading to performance degradation and increased maintenance costs. Thus, the rain erosion test is a crucial evaluation method to assess the durability of coatings, especially for applications exposed to harsh environmental conditions. Referring to ISO/TS 19392–3, rain erosion is assessed by subjecting the surface to high-speed water jets or impacting droplets, reflecting the conditions of droplets hitting wind turbine blade tips at speeds up to ~90 m/s [42] (Fig. 1). This test was carried out for three coated beams for 6000 impacts at 160 m/s, which is higher than the 90 m/s droplet velocity. The higher velocity is used to accelerate damage and ensure reproducible evaluation.

2.4.3. Abrasion resistance

The abrasion resistance of a coating is critical for evaluating its durability against mechanical wear. The abrasion resistance test, performed as per ASTM D4060, involved 1000 cycles of a CS-17 abrasive rotating wheel under a 1 kg load at 60 rpm to simulate mechanical wear on the coating. The measurement of weight loss after 1000 abrasion cycles provides valuable insights into the material's resistance to abrasion, indicating how well the coating can withstand wear under mechanical stress.

2.5. Assessment of coating icephobicity

To comprehensively evaluate the icephobic performance at the laboratory scale, five complementary tests were carried out on the coated surfaces. This includes measuring ice adhesion strength using centrifugal force, performing a push-off test, subjecting the samples to repeated icing/de-icing cycles to assess durability, and determining both the ice nucleation temperature and freezing delay time. This multi-test strategy was not only intended to enhance the accuracy of the study but also to establish correlations among the results, thereby providing deeper insights into the coatings' icephobic behavior.

2.5.1. Ice nucleation temperature

Samples were prepared by applying a thin, uniform layer of the test coatings to Tzero aluminum pans, which were then allowed to dry thoroughly. A 5 mg droplet of deionized water was carefully placed at the center of each coated pan to observe ice nucleation, and the use of three replicates per coating allowed us to determine the average nucleation behavior.

The samples were then subjected to a controlled cooling cycle using a TA Instruments DSC 250. The temperature was decreased from 40 °C to −40 °C at a constant rate of 5 °C/min. During cooling, the ice nucleation temperature (IN_temp), defined as the point at which the water droplet

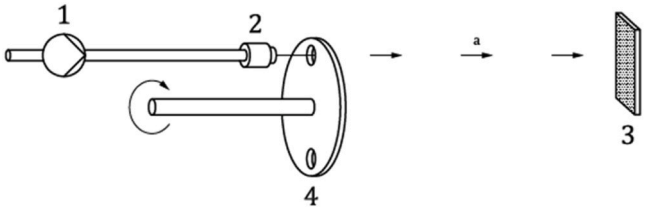

Fig. 1. Schematic of the principle of rain erosion test device (provided by ISO/TS 19392–3:2018); 1: high-pressure pump, 2: jet nozzle, 3: panel holder, 4: rotating disc, a: fluid jet [15].

froze, was identified by an exothermic peak in the DSC thermogram. This temperature, recorded with a precision of ±0.05 °C, was used to evaluate the nucleation behavior of each coating.

2.5.2. Freezing delay time

The freezing delay time was determined by measuring how long a 5 μL water droplet remained unfrozen on coated aluminum coupons. Experiments were conducted at –15 °C using a Krüss™ DSA100 goniometer equipped with a Peltier plate, within a controlled cold chamber. To minimize condensation effects, humidity in the chamber was regulated using anhydrous calcium sulfate desiccants. The final freezing delay time represents the average of five measurements taken from different locations across multiple samples.

2.5.3. Push-off

A custom-made device was used to measure the τice of Gelcoat (VIBRIN G290AA) and Lotus Dry coatings at −10.0 ± 0.2 °C. Fig. 2 shows the setup of the push-off test. Deionized water was poured into a solid plastic cylindrical mold (22 mm in diameter), which was placed on top of aluminum plates coated with the test material (size: 10 × 10 cm^2). The mold stayed in place during freezing and testing to keep the ice in shape and contact area consistently. To make sure the ice fully froze into a solid cylinder, the samples were kept in a cold chamber overnight at −10.0 ± 0.2 °C.

During the test, a fixed probe was used to push the ice cylinder from the side. The probe and load cell (which measures force) stayed still, while the substrate with the ice was slowly pushed horizontally using a worm screw powered by a stepper motor. The speed of movement was 0.5 mm per minute to obtain a quasi-static load. The load cell recorded the pushing force over time.

Before the test began, the height of the probe was carefully adjusted, so it touched the side of the ice just above the coated surface. The highest force recorded (F) before the ice detached was used to calculate the shear adhesion strength using Eq. (1).

$$\tau \text{ ice} = F / A \tag{1}$$

Where A is the area of contact between the ice and the coating. This method makes it easy to repeat the test and get reliable results on how well the coating resists ice sticking.

2.5.4. Icing/De-icing cycles

The durability of the coated surfaces was evaluated by repeating the push-off test 50 times, with τice measured every 5 cycles to monitor performance over time. To ensure consistency, a custom-made plastic mold was used to form ice in a previously determined fixed area on each sample. The mold had a cylindrical cavity with a 22 mm diameter and was positioned using an alignment frame or guide, allowing it to be placed in the same location during each cycle. This setup confined the water to the same spot and ensured that the ice column had a uniform shape and contact area throughout all tests, allowing for accurate and repeatable measurements of ice adhesion.

2.5.5. Centrifugal adhesion test (CAT)

Centrifugal force testing was performed to determine the shear stress required to detach ice samples at a slightly large scale and for more representative atmospheric icing conditions. CAT tests were conducted using aluminum beams (6061-T6 alloy, 340 ×31.8 ×6.4 mm) rotated by an electrical motor.

Two sets of specimens were prepared: one set consisting of aluminum substrates coated with the polyester Gelcoat (VIBRIN G290AA) and a second set coated with the Lotus Dry icephobic coating. Each group included three replicate samples.

To simulate natural icing, all samples were exposed to freezing drizzle (320 μm mean volumetric diameter) at an icing intensity of 11 g/h for 35 min and tested for two temperature conditions: –5 °C and –12 °C, representing glaze and mixed ice formation, respectively [43–45]. During each CAT test, beams were mounted individually in a centrifuge vat and spun from zero up to the ice detachment point at a constant acceleration of 300 rpm/s. To assess centrifugal ice-shedding, the acting force was determined using Eq. (2), taking into account the ice's mass (m), radial position of the center of mass (r), and angular velocity at detachment (ω):

$$F = mr\omega^2 \tag{2}$$

The corresponding centrifugal τice was determined by normalizing this force over the surface area in contact with the ice.

2.5.6. Spinning rotor blade (SRB)

The SRB is a vertical-axis spinning model consisting of a 2000 RPM, 10 hp motor, a 1-inch diameter power steel shaft, a hub, and two blades, with an overall diameter of 0.780 m. The rotating blades are mounted in the Anti-icing Material International Laboratory (AMIL)'s icing wind tunnel, a low-speed facility capable of reproducing cloud conditions with supercooled water droplets. Beyond conventional icing tests, the SRB setup can also be employed for hybrid test configurations, as discussed by Villeneuve et al. [36]. The detailed specifications of the rig are described by Fortin et al. [46]. The spinning rotor blade test [46] allows to study of passive ice protection systems under simulated conditions closer to those encountered in application. The test involves keeping the rotor at a constant rotation speed while exposing it to in-cloud icing conditions. Key ice accretion physics on rotors are captured in the test such as high droplet impact velocity, presence of centrifugal and aerodynamic forces, and efficient dissipation of thermal energy. The test is continued until ice shedding occurs at which point measurements are taken to evaluate τice from Eq. (3):

$$\tau = \frac{\left(\left[m * \left(r - \frac{lc}{2}\right) * \omega^2\right] - [\sigma * e * s]\right)}{lc * S} \tag{3}$$

Where, m: Mass of shed ice, r: Rotor radius (0.391 m), σ: Cohesive normal stress of the ice (1.10 MPa at −5°C (glaze ice) and 1.16 MPa at −10°C (mix ice), values measured for atmospheric ice accretions using method described in [47]), s: Curve length (0.01 m), lc: Ice shedding length (m) (measured after shedding), ω: Rotation speed during icing and shedding (rad/s) (controlled), e: Ice thickness at shedding position (m) (measured after shedding). In the scale-up process of ice adhesion testing, the SRB test marks a turning point where ice failure is no longer fully adhesive. Although the ideal failure scenario for the test is one where the full iced surface area shears off at the lowest ice thickness, in most cases, only a fraction of the ice-covered surface detaches from the blade. The failure mode is mixed where at a specific point, ice will fracture both cohesively through the thickness and adhesively along the interface towards the blade tip.

The coated blade's performance was evaluated against that of uncoated Aluminum blades under controlled experimental conditions at a constant rotational speed of 2000 RPM to obtain similar tip speed than a real V90 wind turbine blade, across two icing scenarios, with ambient temperatures of –5°C and –10°C, as outlined in Table 1.

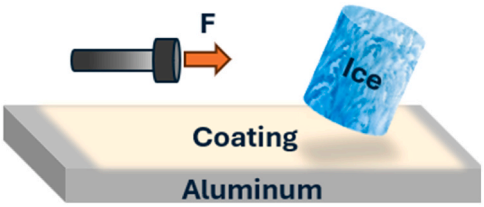

Fig. 2. A schematic of Horizontal push-off test mechanism.

Table 1
Test Conditions for Coating Evaluation at Two Temperatures by the SRB method.

Condition	IWT				SRB			
	Speed m/s	Temperature °C	LWC g/m³	MVD µm	SRB Speed RPM	Blade Tip Speed m/s	Blade Tip speed km/h	Angle of Attack (AOA) °
1	10	-5	0.5	25	2000	80	300	0
2	10	-10	0.5	25	2000	80	300	0

2.5.7. Large scale rotating ice accretion and shedding test bench

Comprehensive lab-scale characterization is essential for establishing a performance baseline for ice protection coatings under controlled and repeatable conditions. While these tests offer high precision and environmental control, they may lack representativity of full-scale operational environments. Bridging this gap is key to evaluating coating performance for wind turbine ice protection and understanding the extent at which it can be efficient to identify future improvement needs. In this study, a large-scale test bench is therefore used to characterize ice shedding with the presence of the coatings in a more representative way and establish a scale-factor correlation of the coating properties to help predict its effect at full scale.

The large-scale test bench is a centrifugal adhesion test bench composed of a horizontal axis 2.6 m diameter rotor equipped with two NACA 0012 blades. Testing is performed in two separate phases. First, the ice is accumulated on the rotor under controlled freezing rain precipitation at a slow rotation speed. Second, precipitation is stopped, and the iced rotor is slowly accelerated at 10 rpm/s until the ice detaches from the blades by centrifugal force. Similar to the procedure described for the SRB in Section 2.5.6, τ_{ice} is determined by subtracting the cohesive portion of the failure from the total centrifugal force acting on the detached ice block. This is achieved by precisely measuring the cohesive fracture surface with a three-dimensional numerical scanner and combining it with the estimated ice cohesion strength to calculate the cohesive force. The adhesive surface area is also obtained using during the scanning process. The estimated cohesive strength of the ice is obtained using a secondary tensile test apparatus [47] under the same experimental conditions. During the icing phase, rotating cylinders are positioned near the rotor to accrete ice simultaneously and a tensile test is used to obtain the corresponding cohesive strength of the ice. The rotor blades can be changed to evaluate different substrates and characterize the performance of different ice protection systems at a larger scale. The rotor stand is installed in a tall cold chamber that includes vibration sensors, temperature probes at four different heights in the chamber, surveillance cameras, high-speed camera and a spraying ramp at the upper most point of the chamber, as depicted in Fig. 3 This system is equipped with numerous protective equipment and enclosed in a protective cage. A spraying system is installed at eleven meters from the

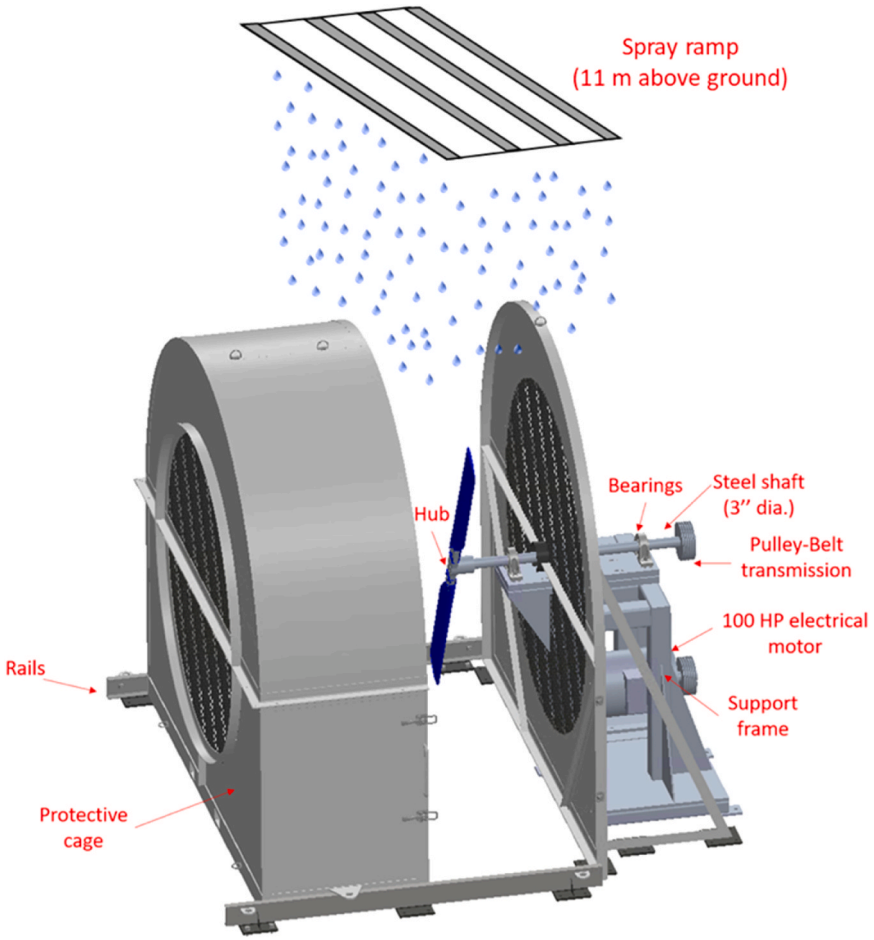

Fig. 3. Diagram of the large-scale test bench inside the cooling chamber.

ground in the cold room to simulate ground atmospheric icing. The system consists of 6 Spraying Systems sprinklers disposed in line to cover the entire width of the rotor from above which can be set to simulate a wide range of icing intensity and droplet MVD. After ice shedding, blades are weighed once more to measure the mass of ice shed and the cohesive and adhesive surface areas of the failure are obtained by 3D scanning. Ice adhesion is then estimated using the same equation presented earlier for the SRB (Eq. 3). Fig. 4 shows an example of ice accumulation on the blades and numerical model of the ice resulting from the three-dimensional scan operation used to measure the ice shape and analyze its type. It also includes the corresponding post-shedding numerical scan, where the highlighted regions clearly indicate the adhesive fracture area, one of the primary areas of interest, along with the much smaller cohesive zone observed at the fracture point.

3. Results and discussion

3.1. Surface characterization

The water contact angle, CAH and sliding angle results are presented in Table 2. The Lotus Dry coating exhibited a contact angle of approximately 100° and a CAH of 10°, classifying it as hydrophobic [48]. In comparison, the reference Gelcoat (VIBRIN G290AA) showed a lower WCA and higher CAH. Although low CAH is an important indicator of ice-repellent behavior and places the Lotus Dry coating within the category of icephobic surfaces [18,49], it alone does not confirm icephobicity. Therefore, further tests are conducted to validate its icephobic performance. This dual classification demonstrates the coating's potential for applications requiring both high hydrophobicity and efficient water shedding.

Table 2
Surface Characterization.

Item Description	Lotus Dry	Gelcoat (VIBRIN G290AA)
WCA	~100° ± 2.2	~ 84° ± 1.9
CAH	~10° ± 1.6	~55° ± 1.2
Sliding angle	~18° ± 0.3	~30° ± 0.4

3.2. Evaluation of the mechanical durability of the coating

3.2.1. Tensile strength

According to the test results presented in Fig. 5, the commercial coating free films behave as a brittle material, fracturing with little to no elastic deformation at both room and –35 °C. The elongation at break was consistently low, averaging 1.25 % at room temperature and 0.53 % at low temperature, both below 2 %, which reflects their limited flexibility. Additionally, the Lotus Dry coating showed low yield strength, averaging 10.9 MPa at room temperature and 8.9 MPa at low temperature. Notably, the Gelcoat (VIBRIN G290AA) could not be characterized by tensile testing due to its extremely fragile nature.

It should be noted that tensile testing of coating free films does not allow direct conclusions about the mechanical performance of the coating when applied to a substrate, as substrate–coating interactions can significantly affect stress distribution, elongation, and overall durability. Nonetheless, these tests provide useful insights into intrinsic coating properties, highlighting potential limitations in elasticity and mechanical strength.

These findings suggest that, while the coating performs better than the Gelcoat (VIBRIN G290AA), it still lacks sufficient elasticity, an essential property for applications involving rotating components such as wind turbine blades. In such systems, coatings must withstand dynamic forces from rotation, vibrations, particle impacts, and environmental stresses. High elongation at break is therefore a key requirement to ensure long-term durability and mechanical reliability.

To address this limitation, future modifications should focus on improving the coating's mechanical strength, with particular attention to enhancing its elongation properties. While improving elongation at break is essential for withstanding mechanical stress from rotation and impacts, it is also important to consider wear resistance. Excessively soft and elastic coatings may degrade faster under environmental exposure and mechanical erosion. A balanced mechanical profile, combining sufficient flexibility to prevent cracking with adequate hardness to resist wear, would be ideal. Therefore, future work should aim to optimize both elongation (>10 %), as suggested in previous studies [18], while maintaining adequate hardness to ensure long-term durability.

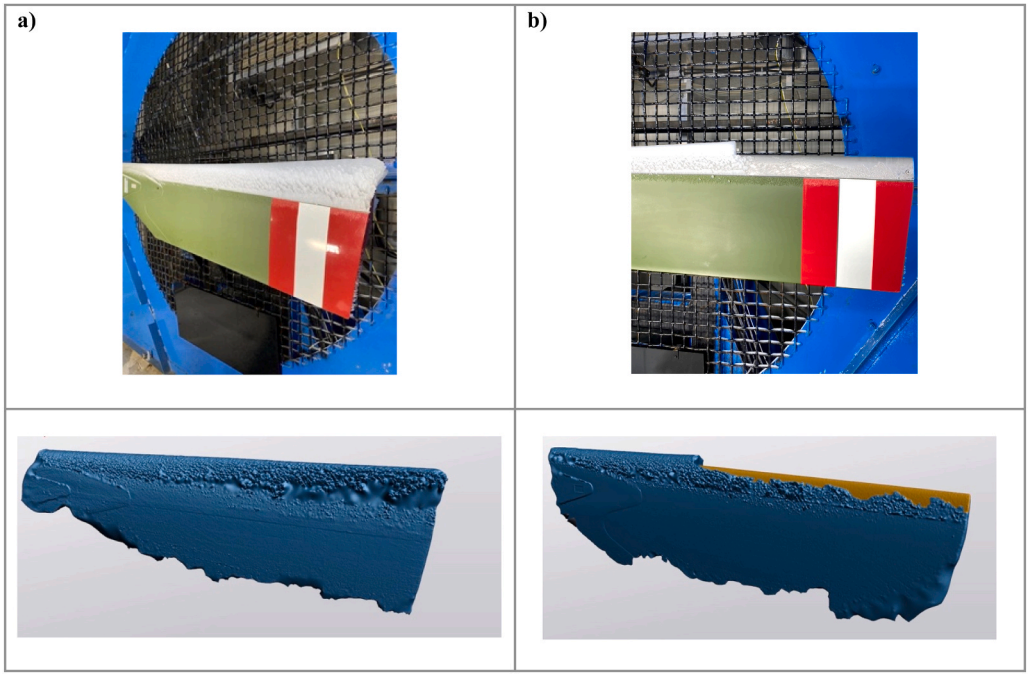

Fig. 4. a) Iced rotor blades after accumulation phase and corresponding numerical model. b) Iced rotor blades after shedding phase and corresponding numerical model with highlighted adhesive fracture area.

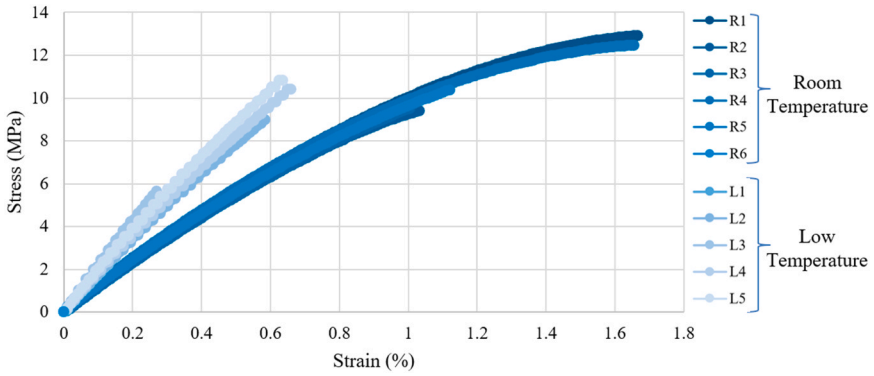

Fig. 5. Tensile Test Results at both room and −40°C temperatures.

Moreover, it is important to mention that the substrate and subtrate-coating systems play an important role in coating' mechanical performance and substrates can control s

3.2.2. Rain erosion

The performance of the commercial coating under rain erosion conditions is summarized in Table 3. According to the standardized evaluation method outlined in ISO-TS-19392–2:2018, the coating qualifies as durable surface, owing to its consistent performance throughout the testing process.

The coating endured over 6000 water droplet impacts at a jet velocity of 160 m/s, simulating the harsh weathering conditions typically faced by wind turbine blades. Notably, no visible surface degradation, delamination, or loss of functionality was observed, as confirmed by unchanged water contact angles (WCA ~ 101° ± 1.3), demonstrating excellent mechanical resilience and surface stability under high-velocity impact.

Although tensile testing revealed that the coating behaves as a brittle material, showing low elongation at break and no plastic deformation, its strong performance under rain-erosion loading indicates that brittle behavior in free-film tension does not directly translate to poor impact resistance when the coating is well adhered to a rigid substrate. In this configuration, the coating's high hardness, scratch resistance, and strong interfacial adhesion allows it to withstand localized, high-velocity impacts. Rather than relying on bulk elasticity, the coating resists damage through sufficient surface toughness, cohesive strength, and the ability of the substrate–coating system to share and redistribute the impact stresses. This contrast highlights that brittleness under uniaxial loading does not necessarily correlate with poor behavior under repeated impact, and that hardness, more than elasticity, is the key property governing resistance to erosive wear. Evaluating coatings under multiple mechanical stress modes therefore remains essential for capturing their true in-service performance.In contrast, the gel-coated reference samples began showing damage before 6000 impacts, including surface wear, micro-cracking, and partial coating removal. This direct comparison highlights the superior erosion resistance of the silicone-epoxy coating, which retained both its structural integrity and functional surface properties after prolonged exposure to aggressive conditions.

These findings suggest that the commercial coating is a promising candidate for long-term application in high-impact environments, such as the leading edges of wind turbine blades. Its ability to withstand repeated mechanical stress without loss of performance enhances its viability as a durable passive icephobic solution, supporting improved operational reliability and reduced maintenance in cold climate energy systems.

The pictures of coated beams after the rain erosion test are presented in Fig. 6:

Table 3
Rain Erosion Test results for both gel-coated and Lotus dry coated samples.

Samples	Number of impacts	Results
Gelcoat (VIBRIN G290AA)	< 6 000	The coating seems to come off the surface in chunks rather than at the precise points of impact
Coating (Gelcoat (VIBRIN G290AA) + Lotus Dry top layer)	> 6 000	No evidence of surface damage

3.2.3. Abrasion Resistance

All three Lotus Dry-coated samples demonstrated excellent abrasion resistance, with an average wear index of 72 mg/1000 cycles and no significant material loss or visible surface degradation after testing (Fig. 7). These results should be interpreted in the context of the unique characteristics of silicone-epoxy systems. Unlike neat, rigid epoxy formulations, silicone–epoxy hybrid coatings are distinguished by their low surface energy and inherent flexibility. Neat epoxy coatings typically exhibit a substantially higher wear index of approximately 115 mg/1000 cycles, indicating a more brittle failure mechanism and greater mass loss [50–52]. The relatively lower wear index of the silicone-epoxy coatings, combined with the absence of delamination or visual degradation, suggests that wear occurs primarily through controlled surface deformation rather than fracture or particle loss. These findings highlight the distinctive wear behavior of silicone-epoxy coatings and their suitability for applications such as wind turbine blades, where coatings are expected to undergo prolonged mechanical stress and environmental exposure while preserving key functional properties.

3.3. Assessment of coating icephobicity

3.3.1. Ice nucleation temperature

Fig. 8 shows that the commercial coating had a lower average ice nucleation temperature (-16.7 ± 0.05 °C) than the reference Gelcoat (VIBRIN G290AA) (-14.5 ± 0.03 °C), based on measurements from three independent samples of each, suggesting delayed ice formation. This behavior can be attributed to its low surface energy, hydrophobicity, and flexible silicone-rich domains, which reduce the likelihood of water molecules organizing into a stable ice nucleus at the interface compared to the more rigid and polar polyester Gelcoat surface. As a result, the coating not only delays ice nucleation but also plays a significant role in minimizing ice accumulation and facilitating ice removal after formation.

3.3.2. Freezing delay time

The silicone-epoxy coating delayed ice formation by approximately 1020 s in a controlled environment at −15 °C, compared to 540 s for the Gelcoat. This prolonged freezing time is a clear indication of the

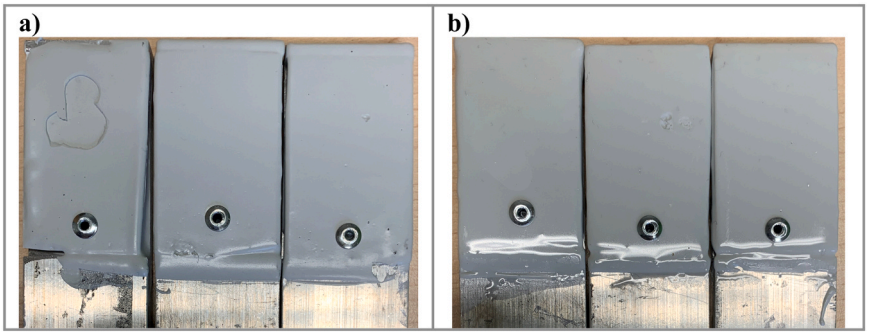

Fig. 6. Rain erosion test results showing the performance of a) the eroded gel-coated surfaces and b) the epoxy-silicone coated sample, which remained non-eroded.

Fig. 7. Surface of the coating after abrasion test, exhibiting minimal wear and no significant damage.

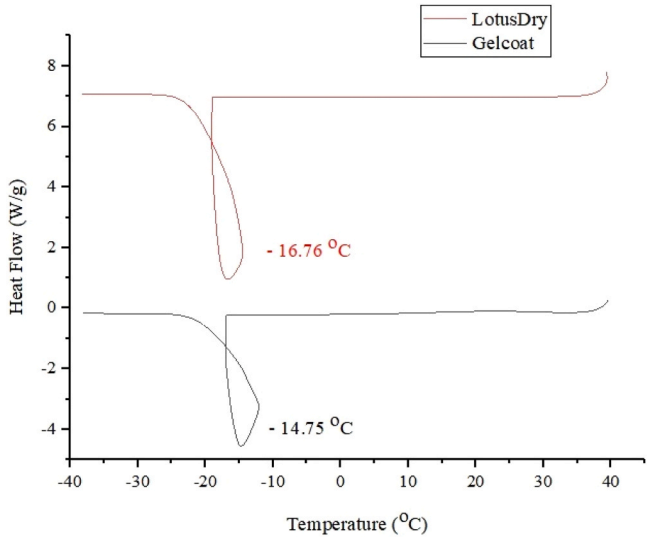

Fig. 8. The average ice nucleation temperatures (INtemp) for the Gelcoat and Lotus Dry coatings.

coating's superior resistance to ice nucleation, which is a critical factor in the development of effective anti-icing surfaces. By impeding the initial formation of ice crystals under subzero conditions, the coating significantly enhances operational reliability and safety, especially in scenarios where ice accumulation can lead to mechanical failure or reduced system performance. The ability to delay freezing not only minimizes the frequency of required maintenance interventions but also contributes to energy savings by reducing the need for active de-icing methods such as heating or chemical treatments. Beyond this improvement, the coating also demonstrates promising anti-icing behavior, as evidenced by its low τice and efficient ice-shedding capability, which are detailed in the following sections. Fig. 9 illustrates the frozen water droplet on the silicone-epoxy coated coupon after 1020 s at −15 °C.

3.3.3. *Push-off adhesion test*

Six substrates were prepared in total, with three coated with Gelcoat (VIBRIN G290AA) and three with Lotus Dry, and τice of an ice mold on each surface was measured using a custom-built push-off test. The Lotus Dry-coated substrates exhibited an average τice of 8.3 ± 1.1 kPa, remaining well below the 20 kPa benchmark [53–55]. In contrast, the gelcoat showed a significantly higher τice of 13.7 ± 3.9 kPa, although still below 20 kPa benchmark. For reference, bare aluminum displayed a much higher τice of 128.9 ± 11.9 kPa. These findings suggest that lateral shear detachment is strongly influenced by surface chemistry. The substantial reduction in push-off force for Lotus Dry-coated samples indicates excellent practical ice-shedding potential, as surfaces with τice values below 20 kPa are typically considered optimal for anti-icing applications [37,56].

3.3.4. *Icing/De-icing cycles by push-off adhesion test*

Throughout 50 icing/de-icing cycles which carried out by a home-made push-off device, the average τice remained consistently low, 19.6 ± 3.6 kPa for the Lotus Dry coating, as illustrated in Fig. 10. The consistently low values of τice (below 20 kPa) observed throughout these tests indicate that the coating's icephobic properties were well-preserved, ensuring reliable performance over extended periods of exposure to icing conditions [57–62]. Notably, the long-term stability and durability of its anti-icing functionality make it well-suited for use on wind turbine blades and other critical outdoor infrastructure exposed to severe winter weather. This reliability can contribute to enhanced operational performance, reduced downtime, and lower maintenance costs, underlining the coating's strong potential for large-scale deployment in cold-climate technologies.

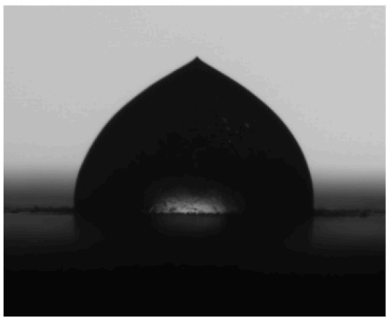

Fig. 9. Frozen water droplet on the surface of the coated coupon after 1020 s at −15°C.

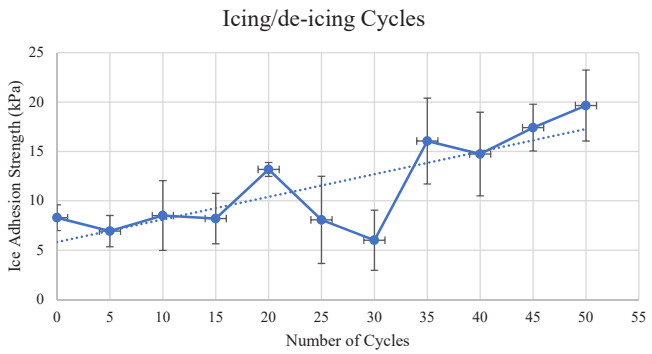

Fig. 10. Ice adhesion strength of the silicone-epoxy coating after 50 icing/de-icing cycles.

3.3.5. *Ice adhesion performance across conditions and test methods*

The different ice adhesion assessment methods presented were tested under two conditions, warmer (−5 °C) and colder (−10 to −12 °C) temperatures. Due to the differences in scale, ice types and ice detachment modes, the comparison of these methods is rendered a complex but hugely insightful analysis. The following section presents the shapes and types of ice obtained at different temperatures for each ice adhesion test as well as the type of detachment for each sample. The test samples appearance is greatly influenced by the precipitation parameters, rotation speed, and the type of fracture that leads to the ice shedding.

Figs. 11 and 12 present result examples for the CAT tests at −12°C and −5°C respectively. For each temperature, a total of 18 repetitions were performed: 6 on aluminum, 6 on gelcoat, and 6 on LotusDry–-coated surfaces. Results at warmer temperatures involve mostly purely adhesive failure, while the second type of failure (cohesive), typically obtained at colder temperatures (Fig. 12). The cohesive failure for aluminum substrates as can be observed in Fig. 11b, while gelcoat and Lotus Dry retained adhesive predominant failure modes (Fig. 11c and d).

Figs. 13 and 14 show ice formation under both conditions and the types of ice shedding for the SRB and large-scale test benches. For the SRB tests, 3 repetitions were performed at –5 °C and 2 repetitions at –10 °C for each of the aluminum and LotusDry–coated blades. Additionally, 6 repetitions at –5 °C and 6 repetitions at –12 °C were conducted for the large-scale tests across all surface types. As shown in Fig. 12a the substrate wettability significantly affected the ice formation process under warmer accumulation conditions, due to the presence of a wet regime, resulting in non-uniform ice growth. This can significantly influence the measured adhesion strength during testing. This was not observed for the large-scale rotor and SRB, probably this is explained by the air flow caused by the rotation, improving dissipation of latent heat and impact ice formation vs ground icing (CAT).

Push-off adhesion failure results were excluded from direct comparison with CAT, SRB, or large-scale tests, as the ice used was molded rather than atmospheric, and the applied strain rate did not reflect the failure conditions of the other tests. Nevertheless, the push-off results are included to provide context, as many studies in the icephobic-coating literature rely on molded-ice adhesion tests to infer performance. By comparing these results with CAT, SRB, and large-scale atmospheric icing measurements, it becomes clear that molded-ice tests do not necessarily predict in-service performance. This highlights a key limitation of relying solely on push-off or molded-ice measurements and underscores the importance of using more representative icing conditions for evaluating coating behavior. Additionally, since the ice studied here was produced while simulating atmospheric accretion, with droplets freezing upon contact, factors such as freezing delay and nucleation temperature are not relevant for this analysis and are also not considered.

A detailed analysis of the ice adhesion data under both conditions reveals distinct performance trends across different substrate types and testing methods, as summarized in Table 4. The following discussions explore the influence of substrate composition, temperature variation, and consistency across testing methods, supported by quantitative comparisons to highlight the reliability and significance of the results.

3.3.5.1. Inter-method correlation and reliability. A comparative analysis of CAT, SRB, and large-scale results reveals key insights into the reliability and representativity of each method. For the aluminum results, SRB and large-scale test values showed significant alignment. When compared to CAT, the SRB and large-scale tests resulted in lower adhesion values, averaging about 58 % lower (SRB) and 57 % lower (large-scale) than CAT results. For instance, at −12°C, CAT measured 0.54 MPa on aluminum, compared with 0.25 MPa for large-scale (a difference of 116 %), while for Gelcoat the gap was even larger (0.47 vs 0.16 MPa, 194 % higher). In contrast, SRB and large-scale results were much closer to each other, differing on average by less than 10 %, which suggests that these two methods yield consistent results as the test is scaled up.

CAT differs in that failures typically involve the complete detachment of ice over a small, well-controlled sample. This keeps the failure mechanism largely strength-dominated, enabling accurate measurement of adhesion strength. Larger-scale configurations such as the SRB and large-scale rotor tests result in a combination of cohesive (through-thickness) and adhesive fracture, since only a portion of the ice sheds while a residual remains attached to the rotating structure. As the scale increases, the failure mechanics transition to being governed by the strain energy dissipation, the presence of flaws and complex stress states.

It is worth noting that these differences are influenced not only by the scale of the setups but also by the geometry of the test specimens. In both the large-scale and SRB tests, ice forms around the curved leading edge of the blade and tends to detach through a mix of adhesive and cohesive failure. In contrast, the CAT test forms ice on a flat surface with a shorter interface, with the adhesion plane parallel to the direction of

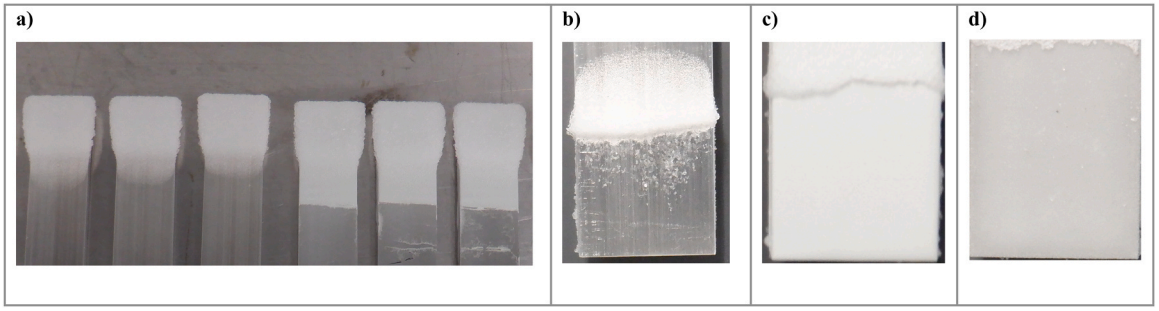

Fig. 11. a) CAT blades ice accumulation in −12ºC on aluminum, gelcoat and Lotus Dry. b) Example of CAT blade result at −12ºC on aluminum showing partial ice detachment c) Example of CAT blade result at −12ºC on gelcoat with minor ice residual. c) CAT blade result in −12ºC on Lotus Dry showing adhesive failure with complete ice detachment.

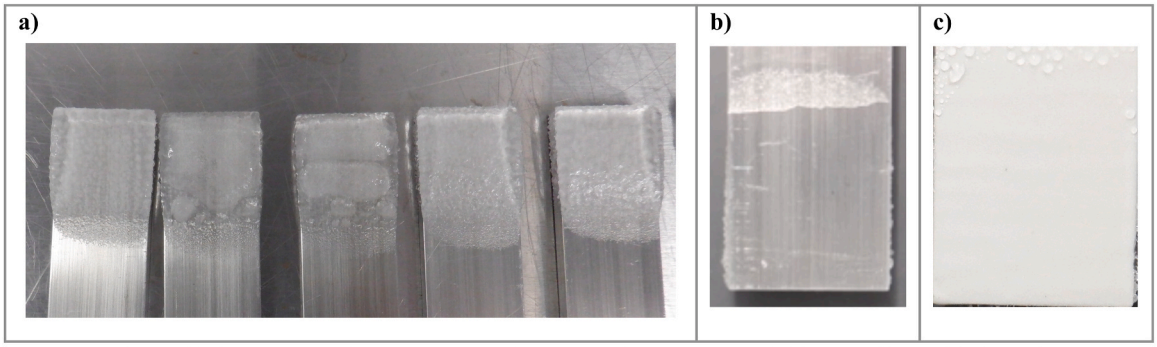

Fig. 12. a) CAT blades ice accumulation in −5°C on aluminum with inconsistent solidification. b) CAT blade result in −5°C on aluminum. C) CAT blade result in −5°C on Lotus Dry with complete ice detachment.

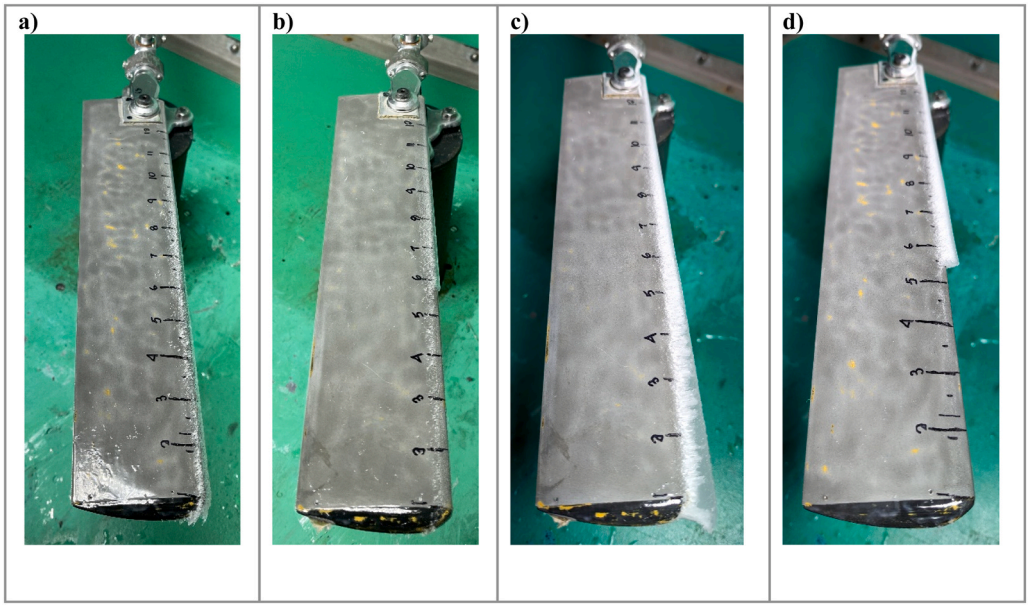

Fig. 13. a) Ice accumulation on SRB blade at −5°C for Lotus Dry. b) SRB test result at −5°C for Lotus Dry, c) Ice accumulation on SRB blades at −12°C on Lotus Dry, d) SRB test result at −12°C on Lotus Dry.

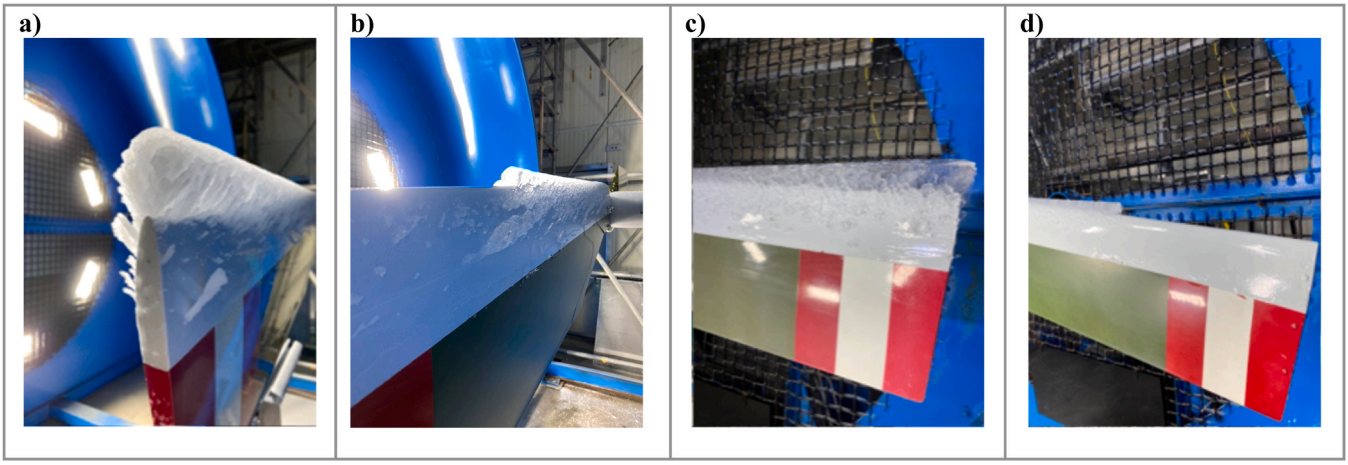

Fig. 14. a) Ice accumulation on Large-scale blade in −12°C on Lotus Dry. b) Large-scale test result in −12°C on Lotus Dry. c)Ice accumulation on Large-scale blade in −5°C on Lotus Dry. d) Large-scale test result in −5°C on Lotus Dry.

spinning, leading more often to purely adhesive failure. In SRB and large-scale methods, it is assumed that at failure, the centrifugal load is equal to the combined adhesive and cohesive limits of the ice acting over the area of the shed piece. However, this assumption neglects fracture

Table 4
Ice adhesion strength of various substrates measured at different temperatures (-5 °C to −12 °C) using multiple testing methods.

Samples	Tests	τ ice at warmer Temperature (-5°C)			τ ice at colder Temperature		
		CAT kPa	SRB kPa	Large-scale kPa	CAT (-12°C) kPa	SRB (-10°C) kPa	Large-scale (-12°C) kPa
Aluminum		290 ± 40	110 ± 2	170 ± 60	540 ± 81[1]	230 ± 30	250 ± 40
Gelcoat		270 ± 50	-	110 ± 10	470 ± 70	-	160 ± 20
Lotus Dry		76 ± 50	27 ± 9	50 ± 30	146 ± 10	101 ± 49	60 ± 30

1.CAT tests at −12°C for aluminum were corrected by removing the cohesive component from the centrifugal force at failure, like the method described for SRB.

mechanics and material defects, where failure may initiate and propagate either within the ice volume or along the interface. This explains why adhesion strength values from SRB and large-scale result in lower values than for CAT as the adhesion force is independent of the surface area of the detached ice block when failure is toughness-controlled. Further investigation into the fracture mechanics of partial ice detachment is needed to establish a more reliable relationship between CAT-measured adhesion strength, the stiffness and tensile strength of ice, and the interfacial fracture toughness, as well as the partial shedding observed on more complex structures. Such work is essential to better predict the timing and location of fracture during ice accretion.

Interestingly, the trends across the three measurement methods are consistent. Using the adhesion reduction factor (ARF), defined here as how many times adhesion on aluminum is higher than on Lotus Dry, Lotus Dry is shown to significantly reduce adhesion. At warmer temperatures, ARF values range from 3.4 to 4.1, indicating that adhesion on aluminum is over three times greater than on Lotus Dry. At colder temperatures, CAT and large-scale tests show ARFs of 3.7 and 4.2, respectively. These consistent reductions suggest that while CAT may better capture adhesion strength as an intrinsic material property, the effect of adhesion reduction is also clearly reflected in the more realistic SRB and large-scale methods.

Large-scale and SRB test benches both have partial shedding of the ice when the rupture point is attained. Because of their difference in size, this behavior can be used to analyse the shedding ratio and extrapolate to build predictions on the behavior of the ice on full scale wind turbines. Table 5 presents a comparison of the ice shed length for both testing methods.

Large-scale and SRB testing differ in their approaches but provide complementary insights. In large-scale testing, ice is accreted to a target thickness at low rotation speeds, after which the speed is gradually increased until shedding occurs. This procedure simulates a wind turbine that has accumulated ice under light wind conditions and later attempts to operate in stronger winds. For passive coatings, the desired performance is early shedding at low rotational speeds combined with high shedding coverage. By contrast, SRB testing involves ice accretion while the blade is already rotating at a constant speed, representing operation in sustained high winds. In this case, shedding occurs once a critical ice mass is reached. For passive coatings, the goal is to minimize the ice mass required to trigger shedding while maximizing the proportion of the blade that sheds.

In terms of shedding behavior, the percentage of shed length is comparable between SRB and large-scale at –12°C. However, at the warmer condition (–5°C), SRB exhibits larger shed lengths. This aligns with the reduction in ice adhesion at warmer temperatures, which facilitates more extensive shedding. The absence of a comparable increase in large-scale testing may be attributed to the delay between ice accretion and centrifugal loading, as well as the greater thermal mass of the larger blades. This delay allows the ice to stabilize at the ambient –5°C. In contrast, SRB testing is more dynamic: the thin aluminum-skinned blades are more susceptible to heating effects, and the latent heat of fusion released during ice accretion can raise the interfacial temperature. As a result, the effective interface temperature in SRB may be higher than in large-scale testing under the same ambient conditions, favoring earlier and more extensive shedding.

For the Lotus Dry coating, its reduced adhesion translates into shedding at lower loads (lower RPM in large-scale and lower accreted mass in SRB). However, shedding lengths are not significantly different from aluminum, suggesting that adhesion alone does not fully dictate the extent of shedding. Shedding typically occurs in the tip-most region of the blade, which is beneficial for the recovery of aerodynamic performance in wind turbine applications. Maximizing shed length while minimizing adhesion strength therefore represents a promising direction for future coating development. Equally important is the need to better understand the stress states that govern ice shedding. The discrepancies observed between adhesion measurements from CAT, SRB, and large-scale methods indicate that mechanical considerations, such as static versus dynamic loading, or partial-shedding (SRB, large-scale) versus complete detachment (CAT), play a key role in the adhesion strength measurements.

Overall, SRB tests offer strong predictive value for field-scale adhesion behavior, particularly when assessing passive coatings under dynamic conditions. Large-scale tests are even more representative but are limited by lower test throughput and higher resource requirements. Meanwhile, CAT remains useful for material screening and assessing temperature effects but may overestimate adhesion due to its simplified loading configuration.

3.3.5.2. Influence of substrate composition. Across all tested substrates, aluminum consistently exhibited the highest adhesion values in CAT, SRB, and large-scale tests. For example, CAT measurements for aluminum increased from 0.290 MPa at −5°C to 0. 54 MPa at −12 °C, highlighting its strong ice-substrate bonding affinity and poor icephobic properties. Notably, CAT cold-condition results for aluminum showed cohesive failure in addition to adhesive failure (partial ice detachement), due to high ice/aluminum adhesion strength. Gelcoat (VIBRIN G290AA) showed slightly lower, yet comparable, adhesion values. On average across all testing methods, the gelcoat demonstrated an adhesion reduction factor (ARF) of 1.35 compared to aluminum.

In contrast, the Lotus Dry-coated surfaces exhibited significantly

Table 5
Ice Shedding Length in Partial Failure Mode Comparison for Large-Scale Tests and SRB Tests on All Substrates.

Temperature (°C)	Substrate	Average Shed Length (mm)		Percentage of blade length shed (%)		Standard Deviation (%)	
		Large-scale	SRB	Large-scale	SRB	Large-scale	SRB
-12	Aluminum	362	89	28 %	28 %	2 %	5 %
	Gelcoat (VIBRIN G290AA)	352	N/A	27 %	N/A	7 %	N/A
	Lotus Dry	366	100	28 %	32 %	17 %	7 %
-5	Aluminum	334	146	26 %	46 %	4 %	5 %
	Gelcoat (VIBRIN G290AA)	388	N/A	30 %	N/A	5 %	N/A
	Lotus Dry	305	126	23 %	40 %	10 %	1 %

lower ice adhesion in all test configurations. CAT results showed adhesion strength of 0.076 MPa at −5 °C and 0.146 MPa at −12 °C, which are significantly lower than both aluminum and gelcoat. Notably, Lotus Dry applied on a gelcoat base layer showed the lowest adhesion under large-scale tests, with values of 0.05 MPa at −5 °C and 0.06 MPa at −12 °C. The average ARF for the Lotus Dry coating was 3.57, confirming its strong potential to significantly reduce ice adhesion on wind turbine blades.

The fact that the ARFs are stable in between test methods and show similar values for substrate comparison highlights the potential of both small scale and scaled-up testing methods and confirms that they can accurately represent substrate behavior without introducing significant error in their performance evaluations. Smaller scale tests are quick and inexpensive, great for screening multiple formulations, and larger scale setups allow to obtain a comprehensive characterisation of well-rounded products, allow to assess durability and act as a last step before field tests.

3.3.5.3. Temperature dependence of ice adhesion. A general trend of increasing adhesion with decreasing temperature was observed, particularly for uncoated substrates, consistent with literature reports of enhanced adhesion at lower temperatures, typically up to a critical point around −20 °C, beyond which adhesion strength may begin to decline [63]. This trend is also influenced by changes in the ice composition: as temperatures move away from 0 °C, glaze ice exhibits stronger adhesion, but this behavior changes as conditions transition toward rime ice, which has different mechanical properties and weaker bonding [64,65]. Additionally, for all substrates tested, a greater variability in ice adhesion results was observed in warmer temperatures, especially on the Large-scale test bench. The greater variability observed at −5°C is attributed to differences in ice morphology and freezing dynamics, but also to a lesser precision for this test bench in the range of lower adhesion values.

Across all testing methods, the average increase in adhesion strength under colder conditions was 1.8 for aluminum, 1.6 for gelcoat, and 2.3 for the Lotus Dry coating. The similar trend observed for gelcoat and aluminum suggests that their adhesion increase with colder temperatures is more characteristic of the ice itself rather than the substrate. In contrast, the stronger temperature dependence observed for Lotus Dry suggests that its surface properties may accentuate thermal effects. Moreover, the Lotus Dry coating demonstrated stable adhesion performance across both tested temperatures, confirming that Lotus-based surfaces maintain consistent ice adhesion and shedding behavior. This supports their temperature-independent anti-icing effectiveness, which is a desirable feature for real-world applications in fluctuating atmospheric conditions.

In both tested conditions, the Lotus Dry is significantly less adhesive than the base substrate for wind turbines. These results support the hypothesis that ice formed at temperatures close to 0°C adheres less and demonstrate that the icephobic coating significantly reduces ice adhesion compared to the gelcoat. In the field, the application of this coating could translate into shorter downtimes for wind turbines. Lower adhesion increases the likelihood of natural ice shedding due to centrifugal forces during rotation or environmental factors such as wind and solar radiation. This passive protection system could enable turbines to resume operation more quickly after icing events or even continue spinning during moderate icing and shedding ice without requiring a complete stop. Furthermore, coatings like this could complement electrothermal de-icing systems by reducing the energy required for ice removal, particularly in areas of the blade where active systems are less efficient. This confirms its potential performance for practical application on wind turbine blades exposed to icing conditions.

4. Conclusion

Ice accumulation on wind turbine blades remains a critical challenge for energy efficiency and reliability. To evaluate how material properties translate into functional performance, our study assessed a commercial silicone–epoxy coating by linking mechanical strength, wettability, and freezing delay to multi-scale ice adhesion tests. Results showed that longer freezing delays and lower contact angle hysteresis correlated with improved icephobicity across push-off, CAT, SRB, and large-scale tests. Differences in adhesion values across test methods were traced to distinct adhesion-dominated versus cohesion-dominated failure behaviors. Adhesion-dominated failures, characterized by clean ice detachment from the surface, are preferable for anti-icing performance and were more frequently observed in CAT and push-off tests. On the other hand, cohesion-dominated failures, which occur within the bulk of the ice, indicate either a stronger interface or the presence of localized stress concentrations. Mixed cohesive–adhesive failures were typically observed in SRB and large-scale measurements, further reflecting the complex nature of ice detachment under realistic conditions. Overall, this study offers an integrated evaluation strategy, combining material-level properties with multi-scale testing to better predict field performance. The consistency between dynamic lab tests and large-scale outcomes validates the coating's icephobicity and underscores the need to consider both interfacial mechanics and scale when designing and evaluating anti-icing coatings. This work represents a significant step toward translating laboratory coatings into field-ready solutions for wind turbines and similar applications.

CRediT authorship contribution statement

Ghazal Minoofar: Writing – review & editing, Writing – original draft, Visualization, Validation, Software, Resources, Methodology, Investigation, Data curation, Conceptualization. **Gelareh Momen**: Writing – review & editing, Writing – original draft, Validation, Supervision, Project administration, Methodology, Investigation, Funding acquisition, Conceptualization. **Thomas Allard**: Writing – review & editing, Writing – original draft, Visualization, Validation, Software, Resources, Methodology, Investigation, Data curation, Conceptualization. **Derek Harvey**: Writing – review & editing, Writing – original draft, Validation, Supervision, Resources, Methodology, Investigation, Data curation, Conceptualization. **Eric Villeneuve**: Writing – review & editing, Writing – original draft, Validation, Supervision, Methodology, Investigation, Conceptualization. **Reza Jafari:** Writing – review & editing, Writing – original draft, Validation, Supervision, Methodology, Investigation, Conceptualization.

Declaration of Competing Interest

The authors declare the following financial interests/personal relationships which may be considered as potential competing interests. Gelareh Momen reports financial support was provided by NSERC - Natural Sciences and Engineering Research Council of Canada-Grant ID: ALLRP 580753–22. Reports a relationship with that includes:. Has patent pending to. If there are other authors, they declare that they have no known competing financial interests or personal relationships that could have appeared to influence the work reported in this paper

Acknowledgements

The authors gratefully acknowledge the support from the Natural Sciences and Engineering Research Council of Canada-Grant ID: ALLRP 580753-22 (NSERC), which funded this research. The authors would also like to acknowledge the Chaire Institutionnelle de Recherche en Matériaux Antigivre Innovants (CiMAGI) at the Université du Québec à Chicoutimi (UQAC) and the Laboratoire International des Matériaux Antigivre (LIMA) for providing the infrastructure necessary to carry out

this work. The authors are especially grateful to Patrice Rondeau of LIMA for his assistance with large-scale testing. Finally, special thanks are extended to Techeol Co. and PRIMA-Québec for their valuable support and collaboration.

Data availability

Data will be made available on request.

References

[1] Hassan Q, et al. The renewable energy role in the global energy Transformations. Renew Energy Focus 2024;48:100545.
[2] Lamraoui F, et al. Atmospheric icing impact on wind turbine production. Cold Reg Sci Technol 2014;100:36–49.
[3] Rodríguez-López MÁ, Cerdá E, Rio Pd. Modeling wind-turbine power curves: effects of environmental temperature on wind energy generation. Energies 2020;13 (18):4941.
[4] Li Y, et al. Scaling method of the rotating blade of a wind turbine for a rime ice wind tunnel test. Energies 2019;12(4):627.
[5] Madi E, et al. A review of integrating ice detection and mitigation for wind turbine blades. Renew Sustain Energy Rev 2019;103:269–81.
[6] Wang L, et al. Wind turbine blade icing risk assessment considering power output predictions based on SCSO-IFCM clustering algorithm. Renew Energy 2024;223: 119969.
[7] Krenn A, et al. Available technologies for wind energy in cold climates. Int Energy Agency Wind Task 2016;19.
[8] Zheng S, et al. Durable waterborne hydrophobic bio-epoxy coating with improved anti-icing and self-cleaning performance. ACS Sustain Chem Eng 2018;7(1):641–9.
[9] Nistal A, Sierra-Martín B, Fernández-Barbero A. On the Durability of Icephobic Coatings: A Review. Materials 2023;17(1):235.
[10] Brassard J-D, et al. Ice accretion, shedding, and melting on cable-stayed bridges: A laboratory performance assessment. Cold Reg Sci Technol 2022;204:103672.
[11] *ISO 527-1:2019 Plastics — Determination of tensile properties, Part 1: General principles*. 2019.
[12] *ASTM D2240*. 2021.
[13] *ASTM D4060-19, 2019*. 2019.
[14] *ISO/TS 19392-6:2023 Paints and varnishes — Coating systems for wind-turbine rotor blades Part 6: Determination and evaluation of ice adhesion using centrifuge*. 2023.
[15] *ISO/TS 19392-3:2018 Paints and varnishes — Coating systems for wind-turbine rotor blades Part 3: Determination and evaluation of resistance to rain erosion using water jet*. 2018.
[16] Geneva, I., *ISO/TS 19392-6:2023 (E); Paints and Varnishes—Coating Systems for Wind-Turbine Rotor Blades—Part 6: Determination and Evaluation of Ice Adhesion Using Centrifuge*. 2023.
[17] Honarkar H, Minoofar G, Barikani M. Effect of the type of anionic center on the characteristics of eco-friendly waterborne polyurethane/acrylate hybrids. Mon FüR ChemChem Mon 2022;153(12):1269–75.
[18] Minoofar G, et al. Progress in icephobic coatings for wind turbine protection: Merging chemical innovation with practical implementation. Crystals 2025;15(2): 139.
[19] Piscitelli F, et al. Superhydrophobic coatings as anti-icing systems for small aircraft. Aerospace 2020;7(1):2.
[20] Zhao Z, et al. Progress in mechanism design of functional composites for anti-ice/deicing materials. Surf Sci Technol 2024;2(1):2.
[21] Nemati Giv A, et al. Effect of reinforcements at different scales on mechanical properties of epoxy adhesives and adhesive joints: a review. J Adhes 2018;94(13): 1082–121.
[22] Ziętkowska K, et al. Transparent Silicone–Epoxy Coatings with Enhanced Icephobic Properties for Photovoltaic Applications. Appl Sci 2023;13(13):7730.
[23] Brusciotti F, et al. Hybrid epoxy–silane coatings for improved corrosion protection of Mg alloy. Corros Sci 2013;67:82–90.
[24] Shamshiri M, Jafari R, Momen G. A novel hybrid anti-icing surface combining an aqueous self-lubricating coating and phase-change materials. Prog Org Coat 2023; 177:107414.
[25] Moghadam SG, et al. In-depth analysis of the effect of physicochemical properties of ionic liquids on anti-icing behavior of silicon based-coatings. Cold Reg Sci Technol 2023;216:104007.
[26] Joseph VS, et al. Silicone/epoxy hybrid resins with tunable mechanical and interfacial properties for additive manufacture of soft robots. Appl Mater Today 2021;22:100979.
[27] Adja AAS, et al. Step by step progress to achieve an icephobic silicone-epoxy hybrid coating: Tailoring matrix composition and additives. J Appl Polym Sci 2023;140 (32):e54262.
[28] Shu T, et al. Anticorrosive and anti-icing/deicing behavior of epoxy composite coatings reinforced with GO-PPy@ SiO2 photothermal fillers. Chem Eng J Adv 2024;18:100592.
[29] Ziętkowska K, et al. Transparent Silicone–Epoxy Coatings with Enhanced Icephobic Properties for Photovoltaic Applications. Appl Sci 2023;13(13):7730.
[30] Zhao L, et al. Icephobic Coating Based on Epoxy/Polydimethylsiloxane Interpenetrating Polymer Network Gel. Coatings 2024;14(1):76.
[31] Sullivan A, Duan X, Yang J. Energy-efficient anti-icing performance of a hybrid superhydrophobic and electrothermal coating on metallic substrates. Mater Chem Phys 2023;301:127700.
[32] Zhang L, et al. Robust photothermal superhydrophobic coatings with dual-size micro/nano structure enhance anti-/de-icing and chemical resistance properties. Chem Eng J 2022;446:137461.
[33] Cheng T, et al. Magnetic particle-based super-hydrophobic coatings with excellent anti-icing and thermoresponsive deicing performance. J Mater Chem A 2015;3(43): 21637–46.
[34] Dhyani A, et al. Surface design strategies for mitigating ice and snow accretion. Matter 2022;5(5):1423–54.
[35] Memon H, et al. Durability enhancement of low ice adhesion polymeric coatings. Prog Org Coat 2021;151:106033.
[36] Villeneuve E, Blackburn C, Volat C. Design and development of an experimental setup of electrically powered spinning rotor blades in icing wind tunnel and preliminary testing with surface coatings as hybrid protection solution. Aerospace 2021;8(4):98.
[37] Rønneberg S, He J, Zhang Z. The need for standards in low ice adhesion surface research: a critical review. J Adhes Sci Technol 2020;34(3):319–47.
[38] Allard T, et al. A Large-Scale Rotor Test Platform for Atmospheric Icing Simulation and Passive Ice Protection Evaluation. Results Eng 2025:108450.
[39] Andrews E, Lockington N. The cohesive and adhesive strength of ice. J Mater Sci 1983;18(5):1455–65.
[40] Ding L, et al. Experimental Study on Adhesive Characteristics of Aircraft Dynamic Icing. Energies 2023;16(13):5037.
[41] Moghadam SG, et al. To be or not to be a hydrophobic matrix? the role of coating hydrophobicity on anti-icing behavior and ions mobility of ionic liquids. Chem Eng J 2024;485:149696.
[42] Ma L, et al. An exploratory study on using Slippery-Liquid-Infused-Porous-Surface (SLIPS) for wind turbine icing mitigation. Renew Energy 2020;162:2344–60.
[43] Godreau, C.F., Paul; Paquet, Yanick; Krenn, Andreas; Wickman, Helena *Technical Report on Ice Detection Guidelines for Wind-Energy Applications*. 2021.
[44] Kraj AG, Bibeau EL. Phases of icing on wind turbine blades characterized by ice accumulation. Renew Energy 2010;35(5):966–72.
[45] Xu Z, et al. A parametric study on the effect of liquid water content and droplet median volume diameter on the ice distribution and anti-icing heat estimation of a wind turbine airfoil. Results Eng 2024;22:102121.
[46] Fortin G, Perron J. Spinning rotor blade tests in icing wind tunnel. 1st AIAA Atmos Space Environ Conf 2009.
[47] Harvey D, Momen G. Dev a Test Appar Meas Tensile Prop Accreted Ice 2024.
[48] Das S, et al. A review on superhydrophobic polymer nanocoatings: recent development and applications. Ind Eng Chem Res 2018;57(8):2727–45.
[49] Li X, et al. Formation of icephobic film from POSS-containing fluorosilicone multi-block methacrylate copolymers. Prog Org Coat 2015;89:150–9.
[50] Palraj S, et al. Corrosion and wear resistance behavior of nano-silica epoxy composite coatings. Prog Org Coat 2015;81:132–9.
[51] Wang X, et al. Mechanical, electrochemical, and durability behavior of graphene nano-platelet loaded epoxy-resin composite coatings. Composites Part B Engineering 2019;176:107103.
[52] Yu Y, Rong MZ, Zhang MQ. Friction and wear of epoxy composites containing silica nanoparticles grafted by hyperbranched aromatic polyamide. Polym Polym Compos 2012;20(8):673–82.
[53] Liu J, et al. Development and evaluation of poly (dimethylsiloxane) based composite coatings for icephobic applications. Surf Coat Technol 2018;349:980–5.
[54] Nistal A, Ruiz-Gonzalez A, Choy K-L. Robust icephobic nanocomposite coatings with superior abrasion resistance. Appl Mater Today 2022;27:101480.
[55] Raman A, et al. Electrospun nanofibers as effective superhydrophobic surfaces: a brief review. Surf Interfaces 2021;24:101140.
[56] He Z, et al. Room temperature characteristics of polymer-based low ice adhesion surfaces. Sci Rep 2017;7(1):42181.
[57] Hejazi V, Sobolev K, Nosonovsky M. From superhydrophobicity to icephobicity: forces and interaction analysis. Sci Rep 2013;3(1):2194.
[58] Khammas R, Koivuluoto H. Durable icephobic slippery liquid-infused porous surfaces (SLIPS) using flame-and cold-spraying. Sustainability 2022;14(14):8422.
[59] Kim JH, et al. Durable ice-lubricating surfaces based on polydimethylsiloxane embedded silicone oil infused silica aerogel. Appl Surf Sci 2020;512:145728.
[60] Laroche A, et al. Silicone nanofilaments grown on aircraft alloys for low ice adhesion. Surf Coat Technol 2021;410:126971.
[61] Qin CC, Mulroney AT, Gupta MC. Anti-icing epoxy resin surface modified by spray coating of PTFE Teflon particles for wind turbine blades. Mater Today Commun 2020;22:100770.
[62] Tuteja A. Designing durable icephobic surfaces. APS March Meet Abstr 2017.
[63] Chen T, et al. Influence of substrate initial temperature on adhesion strength of ice on aluminum alloy. Cold Reg Sci Technol 2018;148:142–7.
[64] Rønneberg S, et al. The effect of ice type on ice adhesion. AIP Adv 2019;9(5).
[65] Shi W, et al. Icing and adhesive characteristics of iced airfoils under rime ice conditions. Coatings 2025;15(5):606.